ACS MATERIALS Au
AN OPEN ACCESS JOURNAL OF THE AMERICAN CHEMICAL SOCIETY

pubs.acs.org/materialsau Article

Expanded Tunability of Intraparticle Frameworks in Spherical Heterostructured Nanoparticles through Substoichiometric Partial Cation Exchange

Sarah K. O'Boyle, Abigail M. Fagan, Benjamin C. Steimle, and Raymond E. Schaak*

Cite This: ACS Mater. Au 2022, 2, 690–698 Read Online

ACCESS | Metrics & More | Article Recommendations | Supporting Information

ABSTRACT: Partial cation exchange reactions provide a synthetic pathway for rationally constructing heterostructured nanoparticles that incorporate different materials at precise locations. Multiple sequential partial cation exchange reactions can produce libraries of exceptionally complex heterostructured nanoparticles, but the first partial exchange reaction is responsible for defining the intraparticle frameworks that persist throughout and help to direct subsequent exchanges. Here, we studied the partial cation exchange behavior of spherical nanoparticles of roxbyite copper sulfide, $Cu_{1.8}S$, with substoichiometric amounts of Zn^{2+}. We observed the formation of ZnS−$Cu_{1.8}$S−ZnS sandwich spheres, which are already well known in this system, as well as ZnS−$Cu_{1.8}$S Janus spheres and $Cu_{1.8}$S−ZnS−$Cu_{1.8}$S central band spheres, which have not been observed previously as significant subpopulations of samples. Aliquots taken during the formation of the heterostructured nanoparticles suggest that substoichiometric amounts of Zn^{2+} limit the number of sites per particle where exchange initiates and/or propagates, thereby helping to define intraparticle frameworks that are different from those observed using excess amounts of exchanging cations. We applied these insights from mixed-population samples to the higher-yield synthesis of ZnS−$Cu_{1.8}$S Janus spheres, as well as the higher-order derivatives ZnS−(CdS−$Cu_{1.8}$S), ZnS−(CdS−ZnS), and ZnS−(CdS−CoS), which have unique features relative to previously reported analogues. These results demonstrate how the diversity of intraparticle frameworks in spherical nanoparticles can be expanded to produce a broader range of downstream heterostructured products.

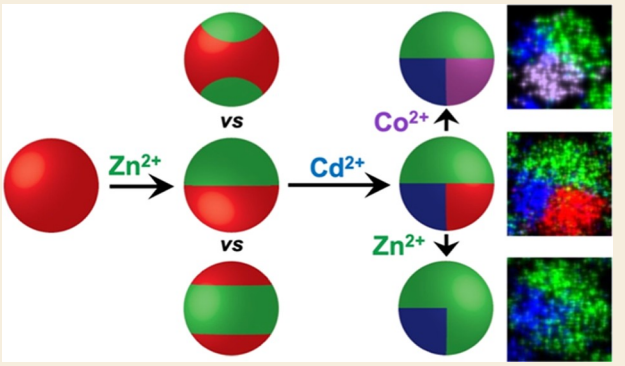

KEYWORDS: *cation exchange, nanoparticles, nanoparticle synthesis, metal sulfides, heterostructures, interfaces*

INTRODUCTION

Heterostructured nanoparticles that incorporate multiple materials in precise locations through well-defined interfaces are useful platforms for both fundamental studies and emerging applications.[1,2] For example, fundamental studies of interface engineering have shown advances in charge separation and enhanced charge transfer in photocatalytic,[3−5] photovoltaic,[6,7] electrocatalytic,[8] and optoelectronic processes,[9] as well as provided tools for tuning photoluminescence behavior.[10−12] From the perspective of applications, these complex heterostructures can be used to improve optoelectronic[13−15] and thermoelectric[16−18] devices. To achieve the desired functions, it is important to control the locations of the materials within a heterostructured nanoparticle and the nature of the interfaces that connect them, including how and where materials are interfaced.

Partial cation exchange reactions provide a powerful synthetic platform for introducing interfaces into nanoparticles while also allowing control over the placement of the constituent materials.[7,19−27] As an example, the Cu^+ cations in roxbyite copper sulfide, $Cu_{1.8}S$, can be replaced with cations such as Zn^{2+} to form ZnS; in this example, two Cu^+ cations are replaced by one Zn^{2+} cation. If only a fraction of the Cu^+ cations is exchanged, heterostructured ZnS−$Cu_{1.8}$S nanoparticles, with one or more interfaces, are formed. These interfaces define the interparticle frameworks that persist throughout subsequent exchanges, keeping the resulting metal sulfide phases separate from one another, even if they otherwise would mix. For example, a subsequent exchange of the Cu^+ cations in ZnS−$Cu_{1.8}$S with Cd^{2+} forms ZnS−CdS[20] despite the miscibility of ZnS and CdS. The interface that typically forms during such partial cation exchange reactions is the one that has the best lattice matching, which for ZnS−$Cu_{1.8}$S is the (001) plane of wurtzite ZnS with the (100) plane

Received: May 13, 2022
Revised: June 9, 2022
Accepted: June 10, 2022
Published: June 28, 2022

https://doi.org/10.1021/acsmaterialsau.2c00038
ACS Mater. Au 2022, 2, 690−698

of roxbyite $Cu_{1.8}S$.[21] The crystal structure relationships between the constituent phases contribute significantly to the interfaces that form upon partial cation exchange and, concomitantly, which region(s) of the nanoparticle each material occupies. Once interfaces are introduced into a nanoparticle through partial cation exchange, *i.e.*, through the transformation of a first-generation (G1) template such as $Cu_{1.8}S$ to a G2 product such as ZnS−$Cu_{1.8}S$, they generally persist through subsequent partial cation exchange reactions, which can be used to incorporate additional materials and interfaces, as described above.[20,25]

By applying up to seven sequential partial cation exchange reactions to roxbyite $Cu_{1.8}S$ nanorods using up to five distinct cations, a library of more than 65,000 unique heterostructured nanorods can now be designed and potentially synthesized.[25] Even in this complex megalibrary, the first partial cation exchange reaction that transforms G1 $Cu_{1.8}S$ nanorods into any of the several G2 derivatives influences the interfaces that form, and therefore, the type of heterostructuring observed, in all downstream, higher-generation products. Similar phenomena are observed for roxbyite $Cu_{1.8}S$ spheres and plates,[20,21] with the first partial cation exchange reaction serving to install the intraparticle interfacial frameworks that define the heterostructuring that is achieved through subsequent partial cation exchange reactions. As an example, partial Zn^{2+} exchange of spherical nanoparticles of roxbyite $Cu_{1.8}S$ produced G2 ZnS−$Cu_{1.8}S$−ZnS.[20−22] A subsequent partial Cd^{2+} exchange of the residual $Cu_{1.8}S$ transformed it to ZnS−(CdS−$Cu_{1.8}S$)−ZnS, a complex heterostructured product having a Janus CdS−$Cu_{1.8}S$ segment sandwiched between two segments of ZnS. A distinct heterostructured nanoparticle isomer, CdS−(ZnS−$Cu_{1.8}S$−ZnS), could be produced by starting with a partial Cd^{2+} exchange reaction that yielded a different interface at the G2 stage.[20,21]

One approach for further diversifying the scope of accessible heterostructured nanoparticles is to expand the types of intraparticle frameworks that can form at the G2 stage, *i.e.*, at the first partial cation exchange of roxbyite $Cu_{1.8}S$. We focus here on the partial cation exchange behavior of spherical nanoparticles of roxbyite $Cu_{1.8}S$ with Zn^{2+} to form heterostructured nanoparticles, which are part of the ZnS/$Cu_{1.8}S$ system that has been targeted previously by our group and others.[19−22,27] Partial cation exchange is often achieved using a significant excess of the exchanging cation and limiting exchange at the diffusion step through reaction time and/or temperature. This is the case for previous reports of spherical ZnS/$Cu_{1.8}S$ heterostructured nanoparticles, such as ZnS−$Cu_{1.8}S$−ZnS, formed through partial cation exchange.[20,22] However, limiting the stoichiometry of the exchanging cations can be used as an alternative to time and temperature to control the extent of cation exchange.[23−25] Here, a substoichiometric amount of the exchanging cation is added to the reaction, allowing the exchange to quickly initiate and propagate relatively uniformly across all nanoparticles in a sample, which also allows heterostructured nanoparticles to form.[24,25,27]

Most studies involving stoichiometrically-controlled partial cation exchange used roxbyite $Cu_{1.8}S$ nanorods. Here, the location and density of the ZnS regions that form within the $Cu_{1.8}S$ nanorods can be controlled by tuning reaction parameters such as Zn^{2+} concentration and temperature, leading to ZnS−$Cu_{1.8}S$ single-tipped nanorods, ZnS−$Cu_{1.8}S$−ZnS double-tipped nanorods, and $Cu_{1.8}S$−ZnS−$Cu_{1.8}S$ central band nanorods.[24,25] The ZnS−$Cu_{1.8}S$−ZnS double-tipped nanorods are analogous to the ZnS−$Cu_{1.8}S$−ZnS sandwich spheres that are well known,[20,22] which emphasizes similarities in the cation exchange behavior of rods *vs* spheres, although ZnS−$Cu_{1.8}S$ and $Cu_{1.8}S$−ZnS−$Cu_{1.8}S$ have not been made as significant subpopulations of spherical nanoparticle systems. It is also known that some partial cation exchange reactions proceed differently on roxbyite $Cu_{1.8}S$ rods *vs* spheres, and these differences motivate comparative studies on rods *vs* spheres. For example, partial Cd^{2+} exchange of roxbyite $Cu_{1.8}S$ spheres produced Janus CdS−$Cu_{1.8}S$ nanoparticles with CdS and $Cu_{1.8}S$ interfaced through the crystallographic planes that have the best lattice matching.[21] In contrast, an analogous partial Cd^{2+} exchange of $Cu_{1.8}S$ rods interfaced CdS and $Cu_{1.8}S$ primarily along a higher-energy crystallographic direction that had significantly poorer lattice matching.[21] The different partial cation exchange behavior of spheres *vs* rods, which led to different intraparticle frameworks, was attributed to the competition between minimizing lattice mismatch *vs* accommodating the increased reactivity and surface energy associated with the nanorod tips.[21] The known similarities and differences in how intraparticle frameworks emerge during partial cation exchange of copper sulfide nanoparticle rods *vs* spheres, as well as the lower diversity of intraparticle frameworks that have been introduced into copper sulfide spheres *vs* rods, motivate additional studies aimed at expanding the diversity of G2 nanoparticle systems and their downstream products.

Accordingly, here, we studied the partial cation exchange behavior of spherical nanoparticles of roxbyite $Cu_{1.8}S$ with substoichiometric amounts of Zn^{2+} so that we could discern generalizable drivers of interface formation that are independent of morphology, *i.e.*, ligand coverage, faceting, etc. Interestingly, we observed spherical analogues of three major ZnS/$Cu_{1.8}S$ heterostructured products that can be made by partial cation exchange of roxbyite $Cu_{1.8}S$ nanorods:[25] ZnS−$Cu_{1.8}S$ and $Cu_{1.8}S$−ZnS−$Cu_{1.8}S$, which have not previously been observed as significant products in spherical nanoparticle samples, and ZnS−$Cu_{1.8}S$−ZnS sandwich spheres, which are well known.[20−22] Aliquot studies using mixed-population samples provided important insights into how the formation of various intraparticle frameworks evolved during partial cation exchange. These insights were then used to achieve a higher-yield synthesis of G2 ZnS−$Cu_{1.8}S$ Janus nanospheres, which means that ZnS−$Cu_{1.8}S$ and ZnS−$Cu_{1.8}S$−ZnS, with distinct intraparticle frameworks, can now be selectively synthesized. We then applied additional partial cation exchange reactions to this G2 ZnS−$Cu_{1.8}S$ Janus nanoparticle to produce several higher-generation derivatives that are distinct from those that could be synthesized using existing G2 templates. The downstream products include ZnS−(CdS−$Cu_{1.8}S$), a G3 heterostructured nanoparticle isomer that is distinct from the previously reported G3 ZnS−(CdS−$Cu_{1.8}S$)−ZnS and CdS−(ZnS−$Cu_{1.8}S$−ZnS) isomers, and from this new G3 isomer, two previously unreported G4 heterostructures, ZnS−(CdS−ZnS) and ZnS−(CdS−CoS). These examples demonstrate how the expanded tunability of G2 intraparticle frameworks influences downstream products that are made through multiple sequential partial cation exchange reactions.

https://doi.org/10.1021/acsmaterialsau.2c00038
ACS Mater. Au 2022, 2, 690−698

EXPERIMENTAL SECTION

Chemical Reagents

Copper(II) chloride [$CuCl_2$, 97%], cobalt(II) chloride [$CoCl_2$, 97%], octadecene [ODE, 90%, technical grade], and di-*tert*-butyl disulfide [DTBDS, 97%] were purchased from Sigma-Aldrich. Zinc chloride [$ZnCl_2$, 99.95%] and cadmium chloride [$CdCl_2$, 99.99%] were purchased from Alfa Aesar. Benzyl ether [BE, 99%] was purchased from Acros Organics. Trioctylphosphine [TOP, >85%] was purchased from TCI America. All solvents (hexanes, isopropyl alcohol [IPA], acetone, and toluene) were of analytical grade. All of the above chemicals were used as received without further purification. Distilled oleylamine [*d*-OLAM] was obtained *via* vacuum distillation of oleylamine [*t*-OLAM, 70%, technical grade, Sigma-Aldrich].[24]

Characterization Methods

Transmission electron microscopy (TEM) images were collected on an FEI Tecnai G20 20 XTWIN microscope operating at 200 kV. High-resolution transmission electron microscopy (HRTEM) images, high-angle annular dark-field scanning transmission electron microscopy (HAADF-STEM) images, and STEM energy-dispersive X-ray spectroscopy (STEM-EDS) elemental maps were collected on an FEI Talos F200X S/TEM at an accelerating voltage of 200 kV. ImageJ software was used to analyze TEM and HRTEM images. Bruker ESPRIT 2 software was used to analyze and generate STEM-EDS elemental map data, where the Cu Kα, Zn Kα, Cd Lα, Co Kα, and S Kα EDS lines were mapped. Powder X-ray diffraction (XRD) data for all materials were collected on an Empyrean diffractometer using Cu Kα radiation.

Synthesis of Spherical $Cu_{1.8}S$ (Roxbyite) Nanoparticles

Spherical roxbyite $Cu_{1.8}S$ nanoparticles were made through modification of a published procedure.[20] Briefly, 341 mg of $CuCl_2$, 47 mL of *d*-OLAM, and 11.8 mL of ODE were combined in a 100 mL 3-neck round-bottom flask equipped with a PFTE-coated magnetic stir bar, a reflux condenser, a gas flow adapter, a thermocouple, and a rubber septum. The mixture was placed under vacuum and heated to 100 °C and held at that temperature for 30 min while stirring. The mixture was then cycled three times with argon gas and placed under argon flow. The temperature was increased to 200 °C, and the mixture was kept at that temperature for 1 h. The temperature was then decreased to 180 °C, and 8 mL of DTBDS (under argon, after three cycles with vacuum and argon) was swiftly injected. The mixture was allowed to stabilize at 180 °C and then sit at that temperature for 15 min before it was cooled to room temperature with a water bath. The black/brown suspension was transferred to centrifuge tubes, and a 1:1 IPA:acetone mixture was added before centrifugation. After decanting, the isolated particles were resuspended in toluene. The addition of 1:1 IPA:acetone, centrifugation, and resuspension in toluene was repeated twice more for a total of three washes. After the final wash, the particles were resuspended in hexanes for storage.

Preparation of Zn^{2+}, Cd^{2+}, and Co^{2+} Exchange Solutions

Separate stock Zn^{2+}, Cd^{2+}, and Co^{2+} exchange solutions were prepared according to published procedures.[25] Briefly, 250 mg of $ZnCl_2$ (or 84 mg of $CdCl_2$ or 56.2 mg of $CoCl_2$), 15 mL of BE, 8 mL of *d*-OLAM, and 2 mL of ODE were combined in a 50 mL 3-neck round-bottom flask equipped with a PFTE-coated magnetic stir bar, a reflux condenser, a gas flow adapter, a thermocouple, and a rubber septum. The mixture was placed under vacuum and heated to 100 °C and held at that temperature for 30 min while stirring. The mixture was then cycled three times with argon gas and placed under argon flow before the temperature was increased to 200 °C. After 30 min of stirring at this temperature, the reaction mixture was allowed to cool to room temperature. The mixture was then transferred to a 40 mL septum-capped vial, cycled three times with argon and vacuum, and placed under argon for storage and use in future exchange reactions. The Zn^{2+} exchange solution was a pale yellow, clear liquid at all relevant temperatures. The Cd^{2+} exchange solution was clear above 60 °C but formed a cloudy solution at room temperature, so it required heating until clear before use in exchange reactions. The Co^{2+} exchange solution is susceptible to oxidation and requires heating above 80 °C, where the red solution will turn blue, indicating the transformation from Co^{3+} to the desired Co^{2+}.

Partial Zn^{2+} Exchange of $Cu_{1.8}S$ (Mixed-Population Product)

Zn^{2+} cation exchange reactions were performed through modification of a published procedure.[24] Briefly, 7.5 mL of BE, 4 mL of *d*-OLAM, and 1 mL of ODE were combined in a 50 mL 3-neck round-bottom flask with a PFTE-coated magnetic stir bar, a reflux condenser, a gas flow adapter, a thermocouple, and a rubber septum. The mixture was placed under vacuum and heated to 100 °C and held at that temperature for 30 min while stirring. Meanwhile, 18 mg of $Cu_{1.8}S$ nanospheres were dried from solution in a septum-capped vial, cycled three times with argon and vacuum, and placed under argon. Then, 1.75 mL of TOP was injected into the vial, followed by three additional argon/vacuum cycles. This $Cu_{1.8}S$/TOP mixture was sonicated for 45 min while the contents of the round-bottom flask were held under vacuum for 30 min at 100 °C. After 30 min, the round-bottom flask was cycled three times with argon and vacuum, placed under an argon blanket, and cooled to 70 °C. As soon as the $Cu_{1.8}S$/TOP suspension was finished sonicating, it was injected into the round-bottom flask. The temperature was allowed to recover to 70 °C, and 0.849 mL of Zn^{2+} exchange solution (exactly enough for a complete exchange) was swiftly injected. The mixture was allowed to stir at 70 °C for 10 min before cooling to room temperature with an ice bath. The light brown suspension was transferred to centrifuge tubes, and a 1:1 IPA:acetone mixture was added before centrifugation. After decanting, the isolated particles were resuspended in toluene. The addition of 1:1 IPA:acetone, centrifugation, and resuspension in toluene was repeated twice more for a total of three washes. After the final wash, the particles were resuspended in hexanes for storage.

Partial Zn^{2+} Exchange of $Cu_{1.8}S$ (Mixture of ZnS–$Cu_{1.8}S$ and $Cu_{1.8}S$–ZnS–$Cu_{1.8}S$)

Exchange products with one ZnS domain either on one side or in the middle were obtained as a mixed product using a modification of the mixed-population Zn^{2+} partial exchange product procedure described above. They differ only in their Zn^{2+} exchange solution injection procedure. Instead of injecting 0.849 mL of Zn^{2+} exchange solution all at once, it was added in portions of 0.170 mL (theoretical 1/5 exchange) with a wait period of 10 min before injecting the next portion. After three injections, the desired mixture was obtained. The same washing and collection procedures were used, as previously described.

Partial Zn^{2+} Exchange of $Cu_{1.8}S$ (Janus ZnS–$Cu_{1.8}S$)

Janus ZnS–$Cu_{1.8}S$ nanospheres were obtained in high yield using a modification of the mixed-population Zn^{2+} partial exchange procedure described above. The volume of Zn^{2+} exchange solution was reduced to 0.425 mL (theoretical 1/2 exchange), the temperature after 30 min at 100 °C was 120 °C instead of 70 °C, and the stirring time after all injections was increased to 20 min. The reaction was cooled and washed, as described previously.

Partial Cd^{2+} Exchange of Janus ZnS–$Cu_{1.8}S$ to Produce ZnS–(CdS–$Cu_{1.8}S$)

ZnS–(CdS–$Cu_{1.8}S$) nanospheres were produced through an additional injection of Cd^{2+} exchange solution after the formation of Janus ZnS–$Cu_{1.8}S$ *in situ*. Before the washing step of the partial Zn^{2+} exchange (Janus ZnS–$Cu_{1.8}S$) procedure, the reaction temperature was decreased to 110 °C, and 0.6 mL of the prepared Cd^{2+} solution was injected. Once injected, the temperature was allowed to recover to 110 °C, and the mixture sat at this temperature for 15 min. The particles were then isolated using the previously described washing procedure.

Co^{2+} Exchange of ZnS–(CdS–$Cu_{1.8}S$) to Produce G4 ZnS–(CdS–CoS)

An additional Co^{2+} exchange of the ZnS–(CdS–$Cu_{1.8}S$) heterostructured nanoparticles was performed to produce G4 ZnS–(CdS–

https://doi.org/10.1021/acsmaterialsau.2c00038
ACS Mater. Au 2022, 2, 690–698

CoS). The previously described partial Cd^{2+} exchange on Janus ZnS−$Cu_{1.8}S$ was used to generate ZnS−(CdS−$Cu_{1.8}S$) *in situ*. After the partial Cd^{2+} exchange, the temperature was decreased to 100 °C, and 1.5 mL of Co^{2+} exchange solution was injected and allowed to react for 20 min to exchange out the rest of the $Cu_{1.8}S$. The particles were then isolated using the previously described washing procedure.

Zn^{2+} Exchange of ZnS−(CdS−$Cu_{1.8}S$) to Produce G4 ZnS−(CdS−ZnS)

Similar to the Co^{2+} exchange, G4 ZnS−(CdS−ZnS) "notch" heterostructures were produced through an additional Zn^{2+} exchange on G3 ZnS−(CdS−$Cu_{1.8}S$). The previously described partial Cd^{2+} exchange on Janus ZnS−$Cu_{1.8}S$ was used to generate ZnS−(CdS−$Cu_{1.8}S$) *in situ*. After the partial Cd^{2+} exchange, the temperature was increased to 120 °C, and 0.4 mL of Zn^{2+} exchange solution was injected and allowed to react for 10 min to exchange out the rest of the $Cu_{1.8}S$. The particles were then isolated using the previously described washing procedure.

RESULTS AND DISCUSSION

Spherical nanoparticles of roxbyite $Cu_{1.8}S$ were synthesized as previously described;[24] XRD and TEM data are shown in Figure S1 of the Supporting Information. Previous studies of partial Zn^{2+} cation exchange of spherical roxbyite nanoparticles were carried out using a significant excess of the exchanging cation, with partial cation exchange being achieved by limiting the extent of cation diffusion through temperature and/or time control.[20−22,24,27] In contrast, and as discussed in the Introduction, we began here by investigating the exchange of the Cu^+ cations in spherical nanoparticles of $Cu_{1.8}S$ with a stoichiometric amount of Zn^{2+}. This amount represents a volume and concentration of the $ZnCl_2$ exchange solution that would deliver approximately the same number of moles of Zn^{2+} required to replace all of the Cu^+, *i.e.*, a 1:2 ratio of Zn^{2+}:Cu^+. As a bridge between the diffusion-limited and stoichiometry-limited pathways and to gain insights into how the reaction progresses, we quenched the reaction after 10 min at the reaction temperature (70 °C), thereby combining both time and stoichiometry limits. In doing so, we created a scenario where the exchange was stoichiometric at maximum but likely would not go to completion. The purpose of this 2-fold reaction control was to maintain a relatively slow conversion from $Cu_{1.8}S$ to ZnS to track the progression of the cation exchange process by removing and quenching aliquots. Similar to exchange reactions carried out with excess metal cation reagents,[20] these early time points serve to identify the range of products that form in a reaction limited by stoichiometry.

Figure 1a shows a HAADF-STEM image of the product isolated from this reaction, along with a STEM-EDS element map in Figure 1b showing the combined signals for Cu Kα (red) and Zn Kα (green). In contrast to previously reported exchange reactions on spherical roxbyite nanoparticles, which produced ZnS−$Cu_{1.8}S$−ZnS,[20,22] three distinct subpopulations were observed here: ZnS−$Cu_{1.8}S$−ZnS sandwich particles, $Cu_{1.8}S$−ZnS−$Cu_{1.8}S$ particles having a central band of ZnS, and ZnS−$Cu_{1.8}S$ Janus particles. Interestingly, these are similar configurations to those observed during substoichiometric Zn^{2+} exchange of roxbyite $Cu_{1.8}S$ nanorods,[25] which suggests that crystallographic relationships dominate over morphology effects, as highlighted in the Introduction. Powder XRD data for this sample, which confirms that both wurtzite ZnS and roxbyite $Cu_{1.8}S$ are present, are shown in Figure S2 of the Supporting Information. It is important to note that some interfaces appear to be curved because there are several

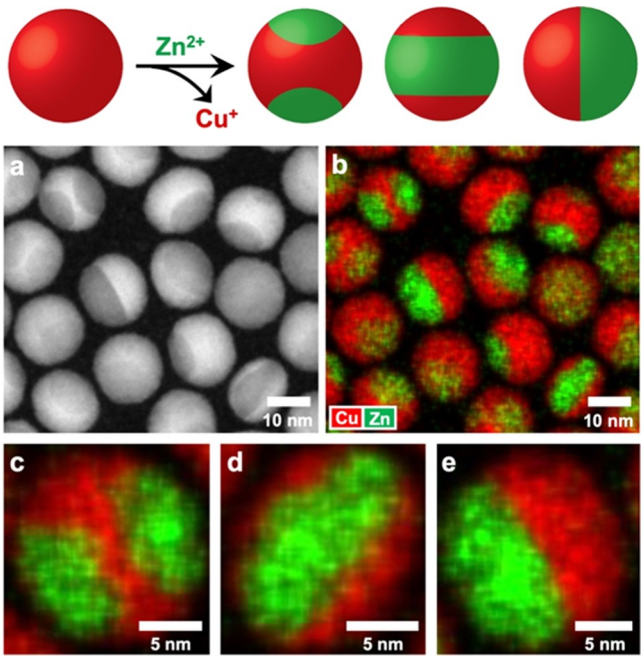

Figure 1. (a) HAADF-STEM image and (b) corresponding EDS element map, where red is Cu Kα and green is Zn Kα for the product of a stoichiometric (1:1 molar ratio) Zn^{2+}−for−Cu^+ cation exchange reaction that was stopped after 10 min. Panels (c−e) show enlarged images of the three observed subpopulations, which include sandwich ZnS−$Cu_{1.8}S$−ZnS particles, inverse sandwich $Cu_{1.8}S$−ZnS−$Cu_{1.8}S$ particles with a ZnS central band, and ZnS−$Cu_{1.8}S$ Janus particles.

crystallographic directions that have similar lattice matching, and therefore, various angled directions can also be favorable.[21,25]

Figure 1c shows an enlarged STEM-EDS element map with combined Cu Kα and Zn Kα signals, as well as the individual element maps, for the ZnS−$Cu_{1.8}S$−ZnS sandwich particles. Before considering the spherical $Cu_{1.8}S$−ZnS−$Cu_{1.8}S$ and ZnS−$Cu_{1.8}S$ particles, it is helpful to review, for the well-known spherical ZnS−$Cu_{1.8}S$−ZnS particles,[22,24] how an analysis of STEM-EDS element maps enables a sandwich particle to be differentiated from other exchange patterns. With spherical particles, there is no preferred orientation when depositing on a TEM grid, so the particles appear in random directions. EDS is a penetrative technique at the size of these nanoparticles, so the elemental maps produced are representative of the entire particle. For ZnS−$Cu_{1.8}S$−ZnS, the absence of Zn signal throughout the middle of the particle is consistent with the true separation of the two ZnS domains and leads to the assignment of this particle as having a sandwich configuration.[20,22] Individual element maps for our mixed-population sample shown in Figure S3 confirm that the ZnS and $Cu_{1.8}S$ regions are segregated. Figure 1d shows analogous STEM-EDS element map data for the $Cu_{1.8}S$−ZnS−$Cu_{1.8}S$ particles, which have a central ZnS band sandwiched between two $Cu_{1.8}S$ regions. As with ZnS−$Cu_{1.8}S$−ZnS, the $Cu_{1.8}S$−ZnS−$Cu_{1.8}S$ configuration can be distinguished from the others due to the lack of Cu signal throughout the middle of the particle in the EDS elemental map. The presence of two separate and nonoverlapping $Cu_{1.8}S$ domains differentiates this type of particle from the others. Finally, Figure 1e shows data for the ZnS−$Cu_{1.8}S$ Janus particles. These particles can be distinguished from the others as they only have one domain of

https://doi.org/10.1021/acsmaterialsau.2c00038
ACS Mater. Au 2022, 2, 690−698

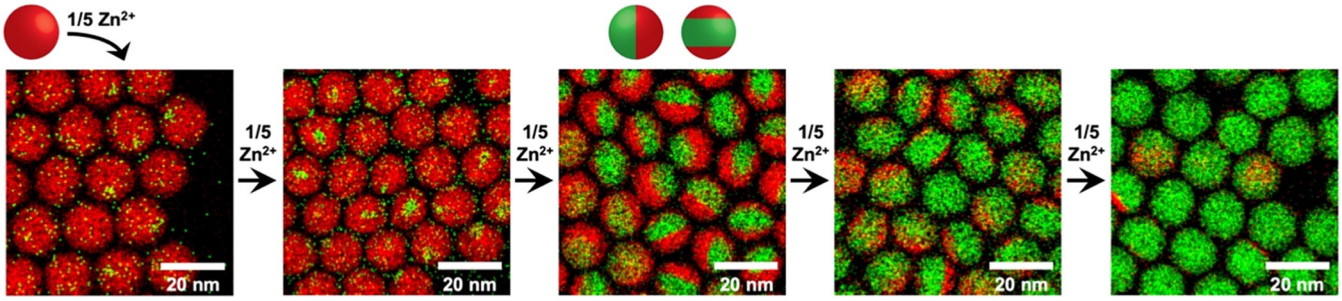

Figure 2. STEM-EDS maps of aliquots taken after each injection of an amount of Zn^{2+} equal to 1/5 of that required to exchange all of the Cu^{+} cations in $Cu_{1.8}S$. Each panel (from left to right), therefore, represents a total of 1/5, 2/5, 3/5, 4/5, and 5/5 (*i.e.*, stoichiometric) exchange accessed through iterative stepwise addition. Both ZnS−$Cu_{1.8}S$ Janus particles and $Cu_{1.8}S$−ZnS−$Cu_{1.8}S$ central band particles are observed. In each STEM-EDS map, red is Cu Kα and green is Zn Kα.

ZnS and one domain of $Cu_{1.8}S$. These latter two particles are particularly interesting as they have not been observed in STEM-EDS maps as partial cation exchange products for spherical particles in the ZnS/$Cu_{1.8}S$ system. For the particles that appear to have overlapping Zn and Cu regions, it is not possible, without advanced imaging using electron tomography, to unambiguously assign a specific exchange product. However, all particles that are observed can be attributed to at least one of the three patterns—sandwich, central band, or Janus—in an orientation where the interface(s) is parallel to the TEM grid. Figure S4 shows each type of particle in various projections to indicate how it will appear on the STEM-EDS maps.

The $Cu_{1.8}S$−ZnS−$Cu_{1.8}S$ central band particles and the ZnS−$Cu_{1.8}S$ Janus particles, which both have only one ZnS region instead of the two in ZnS−$Cu_{1.8}S$−ZnS, likely emerge from the combination of stoichiometrically limited amounts of the exchanging cations (Zn^{2+}) and the short reaction time, both of which may influence the number of sites per particle where exchange initiates and/or propagates. To test this hypothesis and to better understand how these various heterostructured nanoparticles evolve, we conducted an experiment where 1/5 of the stoichiometric amount of Zn^{2+} was added sequentially at set time intervals to allow for the Zn^{2+} to fully react before adding the next 1/5-stoichiometric amount, up to a total of five additions to achieve a complete exchange. The rationale behind this exchange approach was to decrease the favorability of forming two exchange initiation points by severely limiting the amount of Zn^{2+} available while still adding enough over the course of the reaction to produce significant extents of exchange.[25]

Figure 2 shows STEM-EDS element maps of the aliquots taken 10 min after each 1/5 Zn^{2+} exchange fraction was added, just prior to injection of the next fraction. These aliquots support the hypothesis that lower amounts of Zn^{2+} available for exchange result in fewer exchanged domains in the product, as only the central band and Janus particles, which each have one ZnS domain, are seen throughout this experiment. Adding more Zn^{2+} after the initial 1/5 exchange adds to existing ZnS regions rather than forming new ones. These results with sequential addition of the same exchanging cation also suggest that the dual initiation seen with higher stoichiometry and excess reagents,[20,22] which produces spherical ZnS−$Cu_{1.8}S$−ZnS nanoparticles, may result from simultaneous multisite initiation due to higher concentrations of exchanging cations. These results also point to the possibility of a threshold amount of Zn^{2+} exchange that is required for clear segmentation patterns to emerge. As an additional insight, this experiment also confirmed the assumption that once exchange initiates in a particular location to produce an interface, further exchange of that cation will continue to propagate from that existing interface rather than initiating somewhere else. This is an important guideline for translating microscopic observations to scalable syntheses.

Given the insights from Figure 2 into how the various types of heterostructured ZnS/$Cu_{1.8}S$ nanoparticles form and evolve in mixed-population samples, we set out to synthesize, as a representative example, the spherical ZnS−$Cu_{1.8}S$ Janus particles as a higher-yield majority product. Comparing the Janus particles to the central band particles, the primary difference between the two products is in the number of ZnS−$Cu_{1.8}S$ interfaces present; Janus particles have one, and central band particles have two. We rationalized that one interface would be more preferable than two, as it minimizes the number of interfaces and, therefore, the overall interfacial energy of the system. For this reason, a half-stoichiometric Zn^{2+} exchange was carried out at 120 °C (compared to 70 °C for previous exchanges in this study) to favor the formation of the Janus ZnS−$Cu_{1.8}S$ particles, as we hypothesized that the higher temperature would favor the lower energy product that contains only one interface, which is consistent with reaction conditions that yielded ZnS−$Cu_{1.8}S$ *vs* $Cu_{1.8}S$−ZnS−$Cu_{1.8}S$ nanorods.[25] The results of this experiment are shown in Figure 3. Additional images containing more particles can be found in Figure S5, and powder XRD data, confirming the presence of wurtzite ZnS and roxbyite $Cu_{1.8}S$, are shown in Figure S2. Figure S6 shows an HRTEM image of a ZnS−$Cu_{1.8}S$ Janus particle, indicating that the (001) plane of wurtzite ZnS and the (100) plane of roxbyite $Cu_{1.8}S$ form an interface. This interface, which connects ZnS and $Cu_{1.8}S$ along the crystallographic directions having the best lattice matching, is the one observed in ZnS−$Cu_{1.8}S$−ZnS and other ZnS/$Cu_{1.8}S$ heterostructured nanoparticles.[20,21,25] This observation emphasizes that reaction parameters influence the number of interfaces, while the crystallographic relationships influence their orientation.

Sandwich and central band particles are not observed in this sample, based on the analysis of individual STEM-EDS elemental maps and corresponding elemental line scan data. Based on analysis of STEM-EDS element maps of 75 individual particles, of which all are shown in the STEM-EDS maps in Figures 3 and S4, 27% are in the proper orientation to unambiguously assign as Janus particles, and 57% have overlapping Cu and Zn signals that are consistent

https://doi.org/10.1021/acsmaterialsau.2c00038
ACS Mater. Au 2022, 2, 690−698

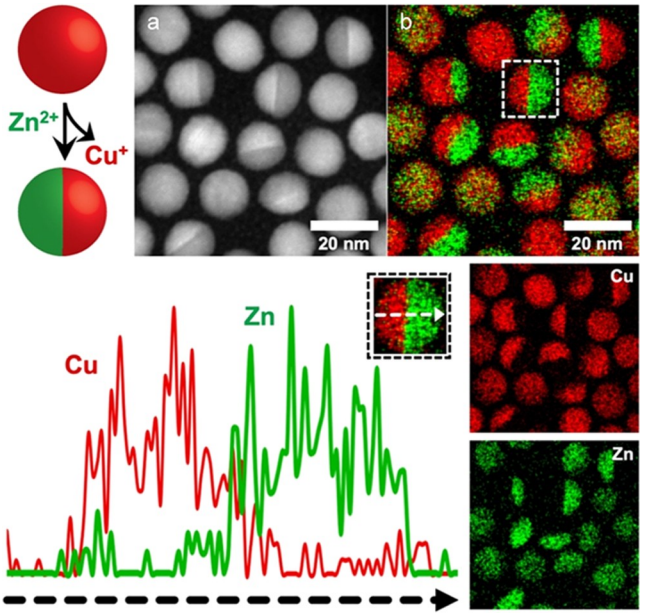

Figure 3. (a) HAADF-STEM image and (b) corresponding EDS map (red is Cu Kα and green is Zn Kα) for the higher-yield synthesis of ZnS−$Cu_{1.8}S$ Janus particles, along with the individual Cu and Zn maps to confirm that the Cu and Zn signals do not overlap. Further confirmation is provided by the line scan across the Janus particle indicated by a dashed box.

with Janus particles but, for the reasons discussed above (and as shown in Figure S4), are not unambiguous. Given the reaction conditions and the lack of any sandwich or central band particles observed among those in different orientations, the particles with overlapping Cu and Zn signals are most likely to be Janus particles, with the caveat that they cannot be unambiguously distinguished from sandwich particles. The remaining 16% of the sample contains unexchanged $Cu_{1.8}S$ particles, which is consistent with the achievable yields of other optimized partial cation exchange reactions.[20,22,24,25]

We next sought to demonstrate how the diversification of G2 heterostructures impacts downstream products, as this capability was a primary motivation for expanding the types of intraparticle frameworks accessible within spherical nanoparticles. We are working with model systems here to demonstrate the concept. However, the ability to precisely place materials, including the metal sulfides accessible through cation exchange of $Cu_{1.8}S$, within a nanoparticle has important implications for future functional targets. For example, photocatalytic architectures require semiconductors and catalysts to be interfaced together in precise configurations, as a targeted configuration will be active while others will not.[27,28] Nanostructures that place PbS, Ag_2S, and surface-modified tellurides at precise locations enable tunable transport properties in thermoelectric nanocomposites.[16] Precisely configured CdS−CdSe−ZnSe heterojunctions produce nanoscopic light-responsive light-emitting diodes.[14] The ability to control where one material is located relative to another within a nanoparticle having multiple materials and interfaces is an important fundamental prerequisite for controlling its properties.

To begin demonstrating how existing cation exchange reactions could be applied to the previously inaccessible G2 template to produce distinct higher-generation heterostructured spherical nanoparticles, we first performed a partial Cd^{2+} exchange on the G2 ZnS−$Cu_{1.8}S$ Janus particles. We replaced approximately half of the remaining Cu^+ to produce the new G3 isomer, ZnS−(CdS−$Cu_{1.8}S$), shown in Figure 4a. As with the G2 particles, various projections of this G3 particle are possible; Figure S7 shows how various projections will appear on the STEM-EDS maps. G3 particles containing ZnS, CdS, and $Cu_{1.8}S$ have been reported previously:[21] ZnS−(CdS−$Cu_{1.8}S$)−ZnS formed from the partial Cd^{2+} exchange of ZnS−

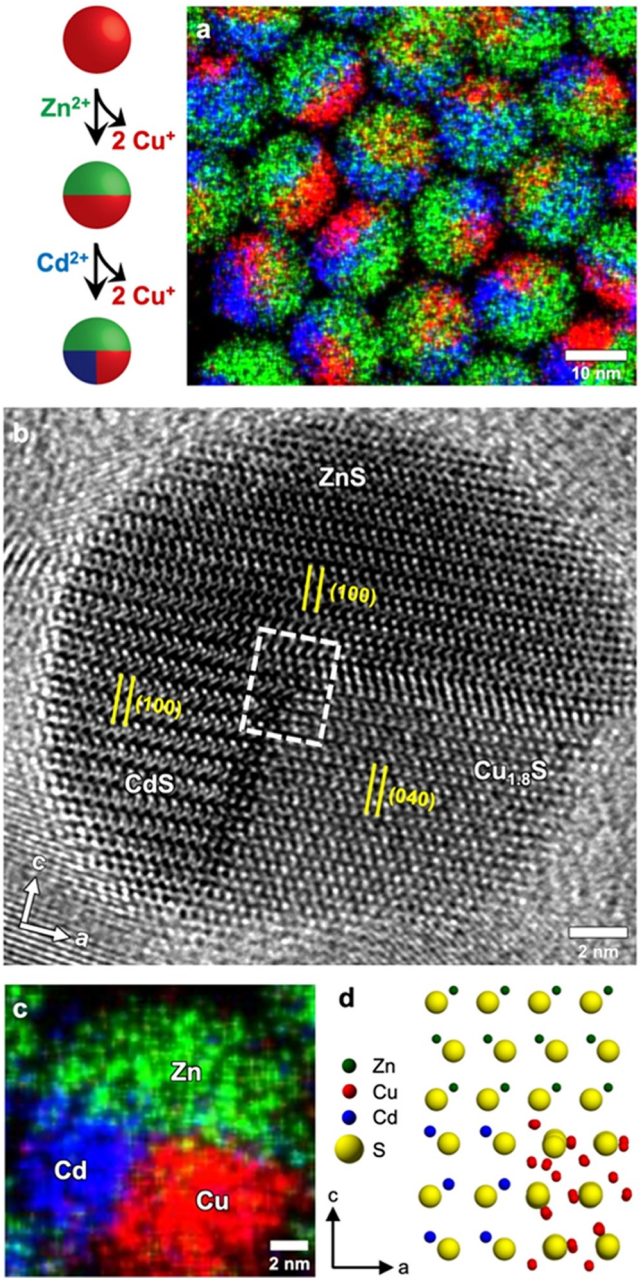

Figure 4. (a) STEM-EDS map for G3 ZnS−(CdS−$Cu_{1.8}S$) made by partial Cd^{2+} exchange of the ZnS−$Cu_{1.8}S$ Janus particles. The spherical nanoparticles lie in different orientations, but a majority of them show evidence that the spatial arrangements of ZnS, CdS, and $Cu_{1.8}S$ match the schematic at the top. (b) HRTEM image and (c) corresponding EDS map for a single ZnS−(CdS−$Cu_{1.8}S$) particle, along with (d) a depiction of the crystallographic orientations at the interfaces corresponding to the boxed-in region in (b). Red is Cu Kα, green is Zn Kα, and blue is Cd Lα.

https://doi.org/10.1021/acsmaterialsau.2c00038
ACS Mater. Au 2022, 2, 690−698

$Cu_{1.8}S$–ZnS, and CdS–(ZnS–$Cu_{1.8}S$–ZnS) formed from the partial Zn^{2+} exchange of CdS–$Cu_{1.8}S$. (Cu^{+} cations are replaced in all cases.) The ZnS–(CdS–$Cu_{1.8}S$) isomer reported here, which requires the G2 ZnS–$Cu_{1.8}S$ Janus nanoparticle to form is distinct. Both previously reported isomers contained one $Cu_{1.8}S$ domain, one CdS domain, and two ZnS domains, while the isomer reported here contains only a single domain of each material. These differences, while subtle, are important for establishing the level of control that is possible in morphologically isotropic spherical nanoparticles by combining partial cation exchange with an expanded set of available intraparticle frameworks.

Analysis of the HRTEM image of the G3 ZnS–(CdS–$Cu_{1.8}S$) heterostructured nanoparticle in Figure 4b, along with the corresponding STEM-EDS element map in Figure 4c, reveals the interfaces that form between the different materials.[20,22,25] It is known that wurtzite CdS and roxbyite $Cu_{1.8}S$ prefer to interface through the CdS (100) and $Cu_{1.8}S$ (010) planes, while wurtzite ZnS and roxbyite $Cu_{1.8}S$ prefer to interface through the ZnS (001) and $Cu_{1.8}S$ (100) planes, as these are the interfaces that minimize lattice mismatch.[20,25,27] Figure 4d shows a depiction of the crystal structure alignments at the interface. The orientation of the interfaces was determined through identification of lattice plane spacings in each material: d_{040} = 3.35 Å for $Cu_{1.8}S$, d_{010} = 4.13 Å for CdS, and d_{010} = 3.81 Å for ZnS. The crystallographic orientations of the interfaces match those of previously reported spherical ZnS/$Cu_{1.8}S$ and CdS/$Cu_{1.8}S$ heterostructured nanoparticles.[21] Taken together, the microscopy data indicate that substoichiometric exchange reactions influence the number of exchanged domains and, concomitantly, the spatial arrangements of the materials but not the crystallographic orientations of the interfaces.

As a final example to further diversify the scope of heterostructured nanoparticles that are now synthetically accessible, we performed additional cation exchange reactions on ZnS–(CdS–$Cu_{1.8}S$) (Figures 5, S8, and S9). In one case,

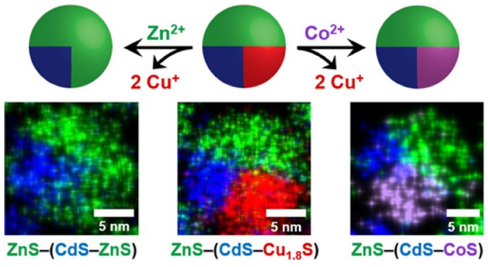

Figure 5. Schematic showing the formation of G4 ZnS–(CdS–ZnS) and ZnS–(CdS–CoS) through partial cation exchange of the G3 ZnS–(CdS–$Cu_{1.8}S$) Janus particles, along with representative EDS maps. Red is Cu Kα, green is Zn Kα, blue is Cd Lα, and purple is Co Kα.

the Cu^{+} cations in the residual $Cu_{1.8}S$ domain were exchanged with more Zn^{2+} to make G4 ZnS–(CdS–ZnS), which produces an asymmetric "notch" of CdS embedded in a ZnS matrix. A different G4 particle was produced from ZnS–(CdS–$Cu_{1.8}S$) by exchanging Cu^{+} in $Cu_{1.8}S$ with Co^{2+} to form ZnS–(CdS–CoS), which has one hemisphere of ZnS and another hemisphere that has CdS on one side and CoS on the other. Powder XRD data confirming the incorporation of each material in the G4 heterostructured nanoparticles are included in Figure S2. For all of these G4 particles, the interfaces defined by the initial Zn^{2+} exchange reaction on spherical G2 $Cu_{1.8}S$ nanoparticles are retained despite having no remaining $Cu_{1.8}S$. These examples demonstrate how increasing the diversity of intraparticle frameworks within spherical nanoparticles expands the library of synthetically accessible heterostructured nanoparticles.

CONCLUSIONS

Substoichiometric Zn^{2+} exchange of the Cu^{+} cations in spherical roxbyite $Cu_{1.8}S$ nanoparticles produces three distinct heterostructured derivatives: ZnS–$Cu_{1.8}S$–ZnS, $Cu_{1.8}S$–ZnS–$Cu_{1.8}S$, and ZnS–$Cu_{1.8}S$. These configurations are analogous to those observed for nanorods,[24,25] although $Cu_{1.8}S$–ZnS–$Cu_{1.8}S$ and ZnS–$Cu_{1.8}S$ have not been previously observed as significant products in spherical nanoparticle systems. These results indicate that guidelines that are well established for nanorods[25] may be transferrable to spherical nanoparticle systems, which is intuitive from a crystal structure perspective since crystal structure relationships determine preferred interfaces. However, this relationship is nonintuitive from a morphology perspective, since nanorods have different faceting and aspect ratios and are known to exchange differently at their tips *vs* along their sides.[21] This study, therefore, bridges the gap between partial exchanges using a significant excess of cations, where the extent of exchange is limited by time and/or temperature and a substoichiometric amount of cations, where the extent of exchange is limited by cation ratios. The G2 nanoparticles observed in this study form because the substoichiometric exchange limits the number of sites per particle where exchange initiates and/or propagates. The ability to control the locations of interfaces and the spatial arrangements of the constituent materials, as shown here, broadens the scope of accessible G2 heterostructured nanoparticles. This capability further diversifies downstream products that are accessible through subsequent partial cation exchange reactions, including G3 and G4 derivatives. Importantly, the insights gained through this study provide additional launch points from which different types of intraparticle frameworks can be integrated into heterostructured nanoparticles, as well as to use them as templates for subsequent reactions. Such capabilities are important for expanding the diversity of heterostructured nanoparticle libraries.

ASSOCIATED CONTENT

Supporting Information

The Supporting Information is available free of charge at https://pubs.acs.org/doi/10.1021/acsmaterialsau.2c00038.

Additional XRD; TEM; HRTEM; HAADF-STEM, and STEM-EDS mapping data (PDF)

AUTHOR INFORMATION

Corresponding Author

Raymond E. Schaak − *Department of Chemistry, Department of Chemical Engineering, and Materials Research Institute, The Pennsylvania State University, University Park, Pennsylvania 16802, United States;* orcid.org/0000-0002-7468-8181; Email: res20@psu.edu

https://doi.org/10.1021/acsmaterialsau.2c00038
ACS Mater. Au 2022, 2, 690−698

Authors

Sarah K. O'Boyle − *Department of Chemistry, The Pennsylvania State University, University Park, Pennsylvania 16802, United States;* orcid.org/0000-0001-8341-9891

Abigail M. Fagan − *Department of Chemistry, The Pennsylvania State University, University Park, Pennsylvania 16802, United States*

Benjamin C. Steimle − *Department of Chemistry, The Pennsylvania State University, University Park, Pennsylvania 16802, United States;* orcid.org/0000-0003-3398-8038

Complete contact information is available at: https://pubs.acs.org/10.1021/acsmaterialsau.2c00038

Notes

The authors declare no competing financial interest.

■ ACKNOWLEDGMENTS

This work was supported by the National Science Foundation under Grant DMR-1904122. TEM, HRTEM, STEM-EDS, and XRD data were acquired at the Materials Characterization Lab of the Penn State Materials Research Institute. S.K.O. also acknowledges Robert Lord and Jennifer Gray for electron microscopy insights and advice, as well as Cameron Holder, Albert Darling, Katherine Plass, Katelyn Baumler, Connor McCormick, and Joseph Veglak for helpful conversations.

■ REFERENCES

(1) Manna, L.; Cheon, J.; Schaak, R. E. Why Do We Care about Studying Transformations in Inorganic Nanocrystals? *Acc. Chem. Res.* **2021**, *54*, 1543−1544.

(2) Enright, M. J.; Cossairt, B. M. Synthesis of Tailor-Made Colloidal Semiconductor Heterostructures. *Chem. Commun.* **2018**, *54*, 7109−7122.

(3) Acharya, K. P.; Khnayzer, R. S.; O'Connor, T.; Diederich, G.; Kirsanova, M.; Klinkova, A.; Roth, D.; Kinder, E.; Imboden, M.; Zamkov, M. The Role of Hole Localization in Sacrificial Hydrogen Production by Semiconductor−Metal Heterostructured Nanocrystals. *Nano Lett.* **2011**, *11*, 2919−2926.

(4) Nakibli, Y.; Mazal, Y.; Dubi, Y.; Wächtler, M.; Amirav, L. Size Matters: Cocatalyst Size Effect on Charge Transfer and Photocatalytic Activity. *Nano Lett.* **2018**, *18*, 357−364.

(5) O'Connor, T.; Panov, M. S.; Mereshchenko, A.; Tarnovsky, A. N.; Lorek, R.; Perera, D.; Diederich, G.; Lambright, S.; Moroz, P.; Zamkov, M. The Effect of the Charge-Separating Interface on Exciton Dynamics in Photocatalytic Colloidal Heteronanocrystals. *ACS Nano* **2012**, *6*, 8156−8165.

(6) Khon, E.; Lambright, K.; Khnayzer, R. S.; Moroz, P.; Perera, D.; Butaeva, E.; Lambright, S.; Castellano, F. N.; Zamkov, M. Improving the Catalytic Activity of Semiconductor Nanocrystals through Selective Domain Etching. *Nano Lett.* **2013**, *13*, 2016−2023.

(7) Zhan, Y.; Shao, Z.; Jiang, T.; Ye, J.; Wu, X.; Zhang, B.; Ding, K.; Wu, D.; Jie, J. Cation Exchange Synthesis of Two-Dimensional Vertical Cu_2S/CdS Heterojunctions for Photovoltaic Device Applications. *J. Mater. Chem. A* **2020**, *8*, 789−796.

(8) Huang, J.; Mensi, M.; Oveisi, E.; Mantella, V.; Buonsanti, R. Structural Sensitivities in Bimetallic Catalysts for Electrochemical CO_2 Reduction Revealed by Ag−Cu Nanodimers. *J. Am. Chem. Soc.* **2019**, *141*, 2490−2499.

(9) Hewa-Kasakarage, N. N.; Kirsanova, M.; Nemchinov, A.; Schmall, N.; El-Khoury, P. Z.; Tarnovsky, A. N.; Zamkov, M. Radiative Recombination of Spatially Extended Excitons in (ZnSe/CdS)/CdS Heterostructured Nanorods. *J. Am. Chem. Soc.* **2009**, *131*, 1328−1334.

(10) Flanagan, J. C.; Keating, L. P.; Kalasad, M. N.; Shim, M. Extending the Spectral Range of Double-Heterojunction Nanorods by Cation Exchange-Induced Alloying. *Chem. Mater.* **2019**, *31*, 9307−9316.

(11) Kroupa, D. M.; Pach, G. F.; Vörös, M.; Giberti, F.; Chernomordik, B. D.; Crisp, R. W.; Nozik, A. J.; Johnson, J. C.; Singh, R.; Klimov, V. I.; Galli, G.; Beard, M. C. Enhanced Multiple Exciton Generation in PbS|CdS Janus-like Heterostructured Nanocrystals. *ACS Nano* **2018**, *12*, 10084−10094.

(12) Li, H.; Brescia, R.; Krahne, R.; Bertoni, G.; Alcocer, M. J. P.; D'Andrea, C.; Scotognella, F.; Tassone, F.; Zanella, M.; De Giorgi, M.; Manna, L. Blue-UV-Emitting ZnSe(Dot)/ZnS(Rod) Core/Shell Nanocrystals Prepared from CdSe/CdS Nanocrystals by Sequential Cation Exchange. *ACS Nano* **2012**, *6*, 1637−1647.

(13) Lu, J.; Shi, Z.; Wang, Y.; Lin, Y.; Zhu, Q.; Tian, Z.; Dai, J.; Wang, S.; Xu, C. Plasmon-Enhanced Electrically Light-Emitting from ZnO Nanorod Arrays/p-GaN Heterostructure Devices. *Sci. Rep.* **2016**, *6*, No. 25645.

(14) Oh, N.; Kim, B. H.; Cho, S.-Y.; Nam, S.; Rogers, S. P.; Jiang, Y.; Flanagan, J. C.; Zhai, Y.; Kim, J.-H.; Lee, J.; Yu, Y.; Cho, Y. K.; Hur, G.; Zhang, J.; Trefonas, P.; Rogers, J. A.; Shim, M. Double-Heterojunction Nanorod Light-Responsive LEDs for Display Applications. *Science* **2017**, *355*, 616−619.

(15) Wen, S.; Liu, Y.; Wang, F.; Lin, G.; Zhou, J.; Shi, B.; Suh, Y. D.; Jin, D. Nanorods with Multidimensional Optical Information beyond the Diffraction Limit. *Nat. Commun.* **2020**, *11*, No. 6047.

(16) Ibáñez, M.; Genç, A.; Hasler, R.; Liu, Y.; Dobrozhan, O.; Nazarenko, O.; de la Mata, M.; Arbiol, J.; Cabot, A.; Kovalenko, M. V. Tuning Transport Properties in Thermoelectric Nanocomposites through Inorganic Ligands and Heterostructured Building Blocks. *ACS Nano* **2019**, *13*, 6572−6580.

(17) Wu, Z.; Chen, X.; Mu, E.; Liu, Y.; Che, Z.; Dun, C.; Sun, F.; Wang, X.; Zhang, Y.; Hu, Z. Lattice Strain Enhances Thermoelectric Properties in Sb_2Te_3/Te Heterostructure. *Adv. Electron. Mater.* **2020**, *6*, No. 1900735.

(18) Zheng, W.; Luo, Y.; Liu, Y.; Shi, J.; Xiong, R.; Wang, Z. Synergistical Tuning Interface Barrier and Phonon Propagation in Au−Sb_2Te_3 Nanoplate for Boosting Thermoelectric Performance. *J. Phys. Chem. Lett.* **2019**, *10*, 4903−4909.

(19) De Trizio, L.; Manna, L. Forging Colloidal Nanostructures via Cation Exchange Reactions. *Chem. Rev.* **2016**, *116*, 10852−10887.

(20) Fenton, J. L.; Steimle, B. C.; Schaak, R. E. Tunable Intraparticle Frameworks for Creating Complex Heterostructured Nanoparticle Libraries. *Science* **2018**, *360*, 513−517.

(21) Fenton, J. L.; Steimle, B. C.; Schaak, R. E. Exploiting Crystallographic Regioselectivity To Engineer Asymmetric Three-Component Colloidal Nanoparticle Isomers Using Partial Cation Exchange Reactions. *J. Am. Chem. Soc.* **2018**, *140*, 6771−6775.

(22) Ha, D.-H.; Caldwell, A. H.; Ward, M. J.; Honrao, S.; Mathew, K.; Hovden, R.; Koker, M. K. A.; Muller, D. A.; Hennig, R. G.; Robinson, R. D. Solid−Solid Phase Transformations Induced through Cation Exchange and Strain in 2D Heterostructured Copper Sulfide Nanocrystals. *Nano Lett.* **2014**, *14*, 7090−7099.

(23) Sadtler, B.; Demchenko, D. O.; Zheng, H.; Hughes, S. M.; Merkle, M. G.; Dahmen, U.; Wang, L.-W.; Alivisatos, A. P. Selective Facet Reactivity during Cation Exchange in Cadmium Sulfide Nanorods. *J. Am. Chem. Soc.* **2009**, *131*, 5285−5293.

(24) Steimle, B. C.; Fagan, A. M.; Butterfield, A. G.; Lord, R. W.; McCormick, C. R.; Di Domizio, G. A.; Schaak, R. E. Experimental Insights into Partial Cation Exchange Reactions for Synthesizing Heterostructured Metal Sulfide Nanocrystals. *Chem. Mater.* **2020**, *32*, 5461−5482.

(25) Steimle, B. C.; Fenton, J. L.; Schaak, R. E. Rational Construction of a Scalable Heterostructured Nanorod Megalibrary. *Science* **2020**, *367*, 418−424.

(26) Zhai, Y.; Flanagan, J. C.; Shim, M. Lattice Strain and Ligand Effects on the Formation of $Cu_{2-X}S$/I-III-VI_2 Nanorod Heterostructures through Partial Cation Exchange. *Chem. Mater.* **2017**, *29*, 6161−6167.

(27) Schaak, R. E.; Steimle, B. C.; Fenton, J. L. Made-to-order Heterostructured Nanoparticle Libraries. *Acc. Chem. Res.* **2020**, *53*, 2558−2568.
(28) Meekins, B. H.; Kamat, P. V. Role of Water Oxidation Catalyst IrO_2 in Shuttling Photogenerated Holes Across TiO_2 Interface. *J. Phys. Chem. Lett.* **2011**, *2*, 2304−2310.

https://doi.org/10.1021/acsmaterialsau.2c00038
ACS Mater. Au 2022, 2, 690−698